Mixed Mode Static and Fatigue Crack Growth in Wind Blade Paste Adhesives

Daniel D. Samborsky, Aaron T. Sears, Pancasatya Agastra and John F. Mandell,
Department of Chemical and Biological Engineering, Montana State University, Bozeman, MT, 59717, USA

Abstract

This study has explored static and fatigue crack growth in thick adhesive joints with fiberglass laminate adherends, for three adhesive systems with a broad range of G_{Ic} values. Test methods include a relatively stiff non-symmetrical cracked lap shear (CLS) geometry as well as more conventional flexural geometries. The several versions of the CLS test geometry allow fully reversed and compression loading, in addition to tension. Flexural test geometries (DCB, MMB, and ENF) have been used to obtain static crack growth properties and as a baseline for comparison to the CLS test results, as well as for comparison to interlaminar growth in the adherends. Crack paths and damage characteristics have been explored using microscopy, for CLS and flexural geometries. Test results are presented for static and fatigue crack growth rates, the latter under tension-tension and reversed loading. Comparisons of the three adhesives are given in terms of crack growth characteristics, static G_{Ic} and mixed mode fracture, and fatigue crack growth resistance.

I. Introduction

Wind turbine blades are large composite structures which are typically resin infusion molded in sections, then adhesively bonded together. The large size coupled with cost constraints result in bond lines at least several mm thick. Blades are subjected to high cycle fatigue conditions under complex loading in service, and many field failures involving bond lines have been reported. While directly applicable test methodologies and data for appropriate adhesives, loadings and geometries have been lacking in the literature, recent studies by the authors have reported test data for strength and fatigue life using simulated blade joint geometries and lap shear type tests[1,2]. The study reported here is an extension crack growth testing, which targets the propagation of existing flaws, and can have the advantage of providing properties which are not limited to a specific geometry. Fracture mechanics based studies of adhesive static and fatigue performance have been reported in the literature, primarily directed toward applications with relatively thin adhesive layers[3].

The challenge is to develop test and analysis methods capable of providing a database of static and fatigue crack growth resistance for thick adhesive joints with a broad range of mechanical properties such as toughness, and which can be applied to structures like blades to predict failure from characteristic flaw types. Most adhesive joints are subjected to mixed mode loading, typically a range of opening (mode I) and shear (mode II) combinations. The potential progression of failure from adhesive flaws into typical types of laminate adherends must also be addressed. Finally, joint performance must be predictable under the broad range of static and fatigue loading conditions experienced by blades in service. The latter requirement means that test methods should be capable of reversed and compressive loading without elastic buckling, a need that is not realized by most adhesives test methods. Test methods which are capable of a full range of mode mixity and, potentially, compressive loading, include the ARCAN[4] and scarf joint[5] geometries, and sub-structural elements like beams[6].

The results of testing must be capable of representation in terms of parameters which can be transferred to geometries like blades. Many representations developed for interlaminar fracture in composite laminates have been adapted to adhesive joints, most notably strain energy release rates (SERR) G_{Ic} (mode I), G_{IIc} (mode II) and combinations of them[3], and the total SERR, G_T (= G_I + G_{II}), usually calculated by the VCCT method[7] in conjunction with finite element analysis[8]. In the case of extensive yielding or damage other methods may be required[5]. Cohesive zone modeling is increasingly applied[10, 11] and global parameters like adhesive/adherend boundary displacements have been used for ductile adhesives[12].

This study has explored several relatively convenient test geometries capable of mixed mode loading under a range of tensile and compressive loading conditions, with typical blade materials. Results have been compared to those from widely used flexural geometries such as mixed mode bending[13], and several analysis options have been explored. The study has included a range of adhesives with differing toughness as well as several adherend laminate surface peel-ply options.

II. Materials and Test Methods

A major focus of the study has involved the development of relatively stiff, thick adhesive cracked lap shear (CLS) specimen geometries capable of fatigue testing under a range of loading conditions from tension-tension (R = 0.1), reversed loading (R = -1) and compression-compression (R = 10), where R is the ratio of minimum to maximum applied load. CLS geometries of this type have been used in earlier adhesives and delamination studies, usually with less thick adherends[9]. Specimen geometries including reinforcement by steel strips (Figure 1) were selected to provide a range of mode mixity dominated by mode II (shear), with a lesser mode I (opening) component, as well as differences in crack stability and local crack path. Initial data from early versions of these tests were presented in Reference 2. The CLS geometry pictured in Figure 1 is both stiff and nonsymmetrical, and gripping conditions are not precisely defined. The massive hydraulic grips and lateral constraints on grip movement[1] resulted in minimal lateral movement of the grips under load; video imaging showed less than 0.2 mm lateral movement where the specimen leaves the grip, at maximum load. Static CLS tests were conducted at a displacement rate of 1.5 mm/min, while fatigue tests were conducted under load control at 1-4 Hz.

Additional static tests were conducted using more standard bending based geometries including double cantilever beam (DCB, ASTM D5528) for pure opening mode, mixed mode bending (MMB) for combined modes I and II[13] and end notched flexure (ENF) for pure mode II[1]. Figure 2 gives the flexure based geometries; the static flexure based tests were conducted with displacement rates of 0.5 mm/min (DCB) and 2.54 mm/min (ENF, MMB). While the flexure based geometries can be loaded in fatigue[3], a full range of loading conditions is difficult to achieve in practice. As discussed later, the flexure based geometries have deformation patterns and far-field stresses which are different from thick composite structures like wind blades, despite similar conditions very close to the crack tip. Adhesives may develop damage zones (yielding and/or micro-cracking) well ahead of the crack tip, where the far-field stress patterns are important[8,12].

The primary adhesive is epoxy based Momentive EP135G3/EKH137G (ADH-1), a relatively brittle system which contains short glass fibers. Limited results are also presented for two tougher epoxy based systems: 3M W1100 (ADH-6) Rhino 405 (ADH-5); the ADH designations are referenced to the SNL/MSU/DOE Fatigue Database where a complete dataset will be available[14]. The adhesives as applied in this study are highly viscous for compatibility with the challenging requirements of bonding large blades; when mixed and applied, they contained significant levels of widely distributed small pores, as well as occasional larger pores up to a cm in size. The laminate adherends are infused UD glass fabric Vectorply ELT-5500, which contains a low content of transverse strand backing[1], with epoxy resin Momentive RIMR135/RIMH1366, 58% fiber by volume. Laminates were four plies thick except for several flexural geometries which used three plies; ply thickness is approximately 1.3 mm. The bonded laminate surfaces were the 0^o side of the fabric (as opposed to the backing side) with direct peel-ply (no abrasion)[1]. The peel ply used in most cases was Airtech Release Ply Super F, with comparison data presented for Econo Ply E and Econo Ply J.

Bonded joint specimens were machined from a sandwich construction[1,2]. The two part adhesives were either hand mixed with a trowel or machine mixed using a Dac150.1FVZ Speed Mixer for 4 minutes at 1500 RPM. The mixed adhesive was applied to each surface with a trowel, then the two laminate sides were assembled into a sandwich. Curing was at room temperature for 24 hours followed by 8 hours at 70^oC. Test coupon strips were then machined from the sandwiches and notches for the CLS geometries were also machined, with care to not penetrate the opposite laminate surface.

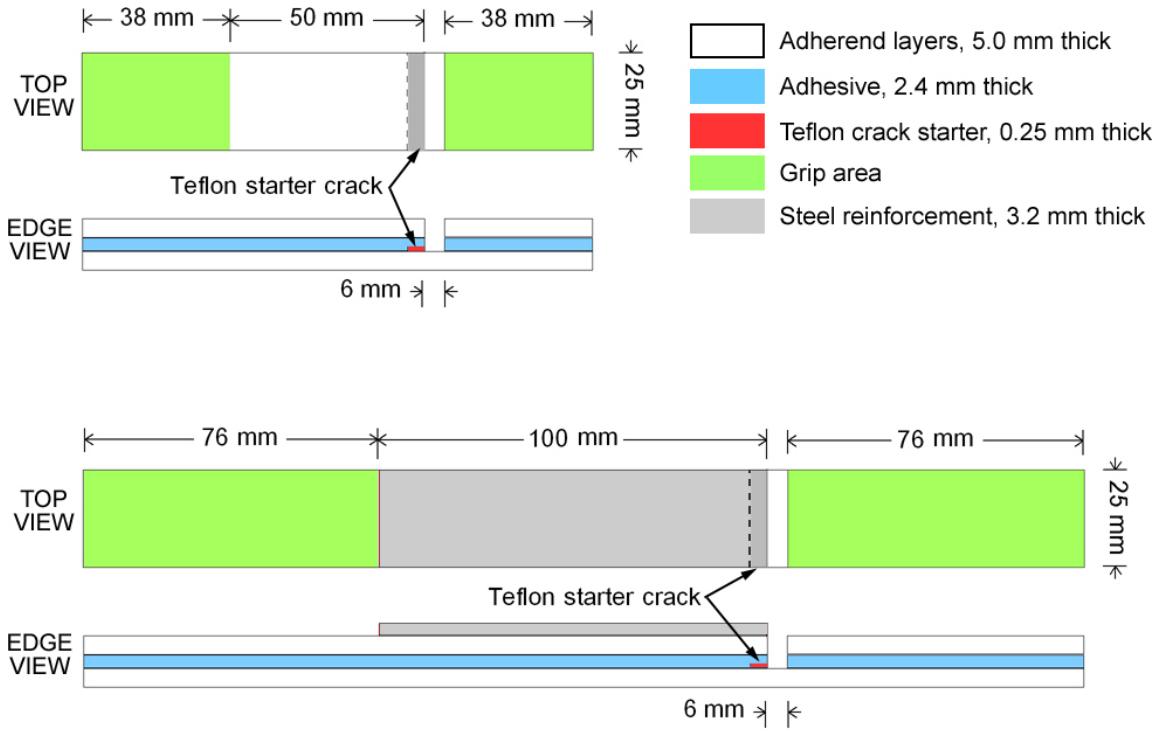

1(a). Coupon dimensions: top, short coupon with 50 mm gage length; bottom, 100 mm length specimen showing added steel reinforcement.

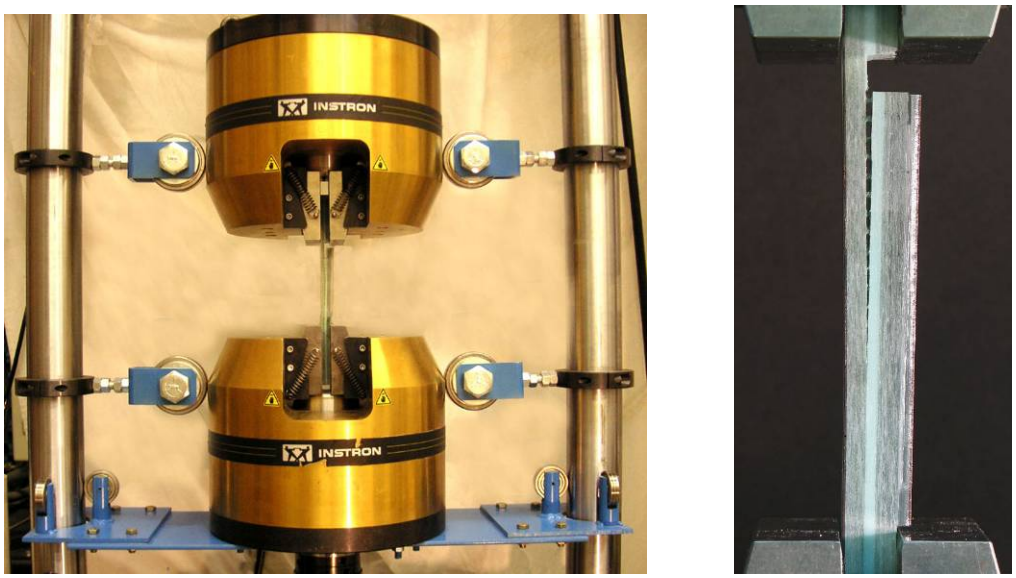

1(b). Test set-up with long specimen shown under load.

Figure 1. Cracked lap shear (CLS) Specimen (a) schematics and (b) photos of test set-up.

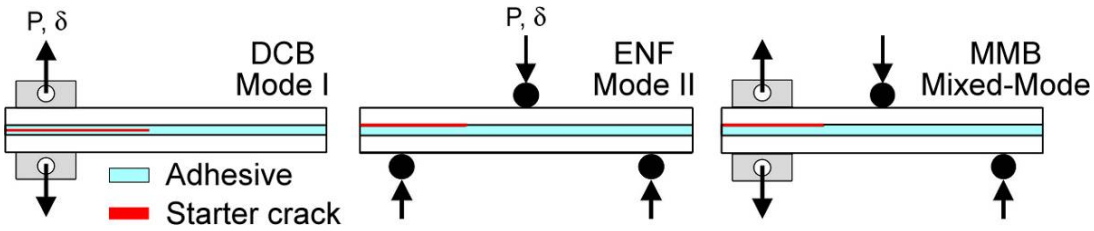

Figure 2. Flexural test geometries showing starter crack positions in adhesive: DCB, center or top; ENF, top; MMB, top.

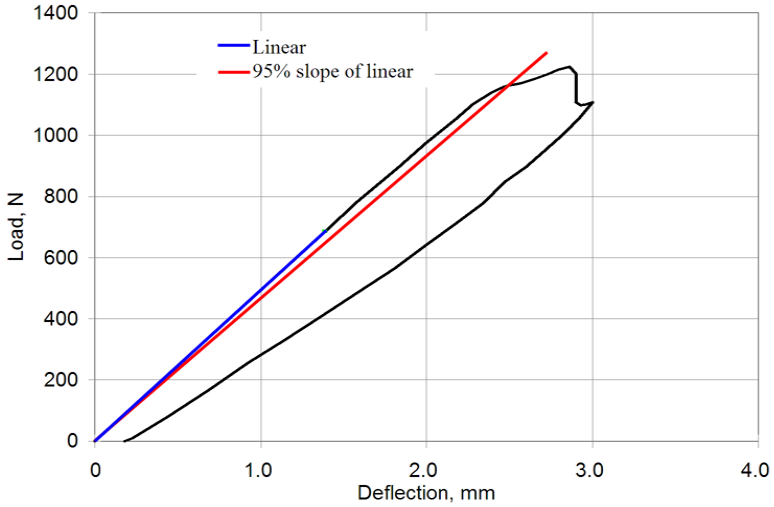

Figure 3. Typical load versus actuator displacement curve and critical load determination for an MMB specimen.

Calculation of SERR's for the flexural-type specimens (Figure 2) followed the description in Reference 1 for ply delamination tests, ignoring the contribution of the adhesive to the stiffness or dimensions; results are compared to more detailed FEA analysis described later. Measured laminate properties used for these calculations are given for the laminates below; the adhesive properties for FEA analysis were taken from Reference 1 as E = 2.76 GPa and ν = 0.35. Critical loads were determined by the offset method illustrated in Figure 3. The critical strain energy release rate to grow a crack in the material can be obtained by the use of the load versus displacement curve of the test (Figure 3) and the modified beam theory (MBT) method[1]. For mode I, DCB:

$$G_{Ic} = \frac{3P\delta}{2ba} \tag{1}$$

where: P = critical load at crack propagation
δ = displacement between DCB cantilever arms at critical load
b = specimen width (25 mm nominal)
a = crack length measured from the center of the load pins

For Mode II, ENF[15]:

$$G_{IIC} = \frac{9P^2a^2C}{2b(2L^3 + 3a^3)} \tag{2}$$

where: P = critical load at propagation
a = initial crack length measured from support point
b = specimen width (25 mm nominal)

C = specimen compliance (= center point deflection/P)
L = one-half support spacing distance

For the mixed mode bending (MMB) test (Figure 4)[1, 13]:

$$G_I = \frac{12P_I^2}{b^2h^3E_{11}}\left(a_o^2 + \frac{2a_o}{\lambda} + \frac{1}{\lambda^2} + \frac{h^2E_{11}}{10G_{13}}\right) \tag{3}$$

$$G_{II} = \frac{9P_{II}^2}{16b^2h^3E_{11}}\left(a_o^2 + \frac{h^2E_{11}}{5G_{13}}\right) \tag{4}$$

$$\lambda = \frac{1}{h}\sqrt[4]{\frac{6E_{22}}{E_{11}}} \tag{5}$$

$$P_I = P_C\left(\frac{3c - L}{4L}\right) \tag{6}$$

$$P_{II} = P_C\left(\frac{c + L}{L}\right) \tag{7}$$

where,
a_o = initial crack length
b = width of specimen (25 mm nominal)
c = geometric variable that changes the G_I/G_{II} ratio
E_{11}, E_{22} = longitudinal and transverse moduli, taken as 45.8 MPa and 8.33 GPa, respectively
G_{13} = in-plane shear modulus, taken as 8.55 GPa
G_I, G_{II} = strain energy release rate in mode I and II, respectively
h = laminate thickness (5.0 mm nominal, doesn't include adhesive thickness)
L = half-length of the bottom support
P_C = critical loading determined from load-deflection curve
P_I, P_{II} = mode I and II loadings, respectively
λ = elastic foundation correction
See the illustration of the apparatus in Figure 4 for the geometric variables a_o, c, h and L. Lambda is the parameter in the elastic foundation correction and is a function of h, E_{11} and E_{22}.

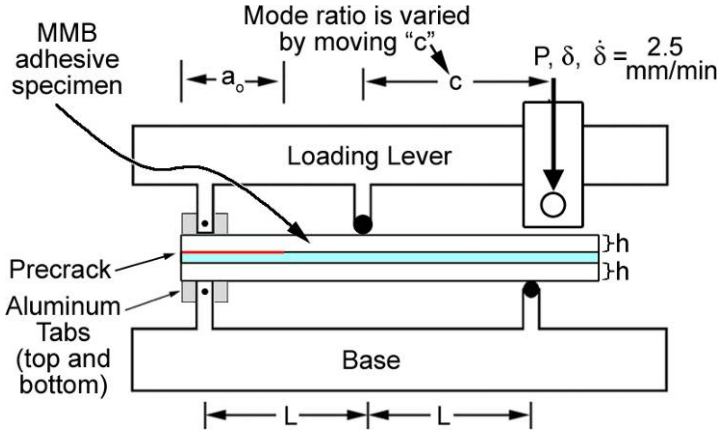

Figure 4. Mixed mode bending apparatus and specimen.

III. Crack Propagation Paths and Stability

Crack paths in adhesive joints are recognized[3] to vary depending on overall geometry, far field stresses (T-stresses), and adhesive, adherend and interface properties. Cracks do not necessarily follow the path of least resistance[3], as observed in this study, discussed later. Simulated wind blade joints[1] and actual wind blade failures are typically characterized by cracks starting in the adhesive layer, and then transitioning to interlaminar cracks in adjacent laminates. A transition from the adhesive into the laminate (through the first ply) is shown in Figure 5 for a static crack in a symmetric version of the long CLS specimen with steel reinforcement; this was the only geometry where a transition into the laminate interior was observed for the thick unidirectional fabric used in this study. The laminate adherends selected for this study were intended to reduce the tendency for the crack to transition into the laminate, to allow study of adhesive and interface failure. In particular, thick unidirectional fabric was used as contrasted with less thick off-axis fabrics like biax[1]. Actual wind blades often bond to biax layers, so there would be a greater tendency of cracks to transition into the laminate than for the tests reported here. The topic of mixed mode interlaminar cracks with this class of laminate is discussed briefly, later. The major transition from adhesive to interior laminate is in addition to more localized crack path transitions from cohesive in the adhesive to the laminate fabric interface. These crack path transitions were always associated with unstable jumps or arrests of the crack in this study.

Crack paths and crack path transitions observed in this study are illustrated in Figure 6, on sections parallel and transverse to the crack growth direction. Cracks in the baseline adhesive, ADH-1, tended to grow inside the adhesive, but associated with the peel-ply surface of the laminate resin, path B. Shown at several stages of development in Figure 7, the crack tip area gradually formed from micro-cracks initiating at peel ply features, pores, and short adhesive fibers, over a zone about 0.2 to 0.4 mm length, then merging into a continuous crack over 1-2 mm ahead of where complete crack opening and sliding appeared possible. The extensive porosity is evident in the micrographs. ADH-1 cracks in this path were stable, growing slowly in static or fatigue tests for the CLS geometries. Often, the entire 100 mm crack length for CLS specimens with steel reinforcement (Fig. 1), and 50 mm crack length for short CLS specimens without steel, would show this path, although rare transitions to path C were observed (Figure 8, bottom). The crack stability for these CLS geometries satisfied the major requirement for the study of mixed mode crack propagation. Other geometries such as the long CLS specimen without steel reinforcement, and a symmetrical CLS geometry with two adhesive layers, produced frequent unstable crack jumps to path C for adhesive ADH-1 under both static and fatigue loading. Cracks in the DCB, MMB and ENF geometries also became unstable after a few mm of growth, transitioning from path B to path C (Figure 9), with the ENF geometry showing the greatest extent of stable growth (Figure 8, top), about 10 mm.

Damage along and ahead of the cracks in adhesive ADH-1 (Figs. 7 and 8) is typical of hackle formation commonly observed for mixed mode and mode II delamination cracks in brittle resin laminates[16]. While the thick adhesive allows hackle-like features associated with the crack, which are relatively large (0.1-0.3 mm deep) compared to those possible with thin adhesive layers or interlaminar regions in most composites, the damage was localized to a small fraction of the total adhesive thickness for path B cracks. Occasional larger zones of crack kinking were observed for unstable cracks on path C.

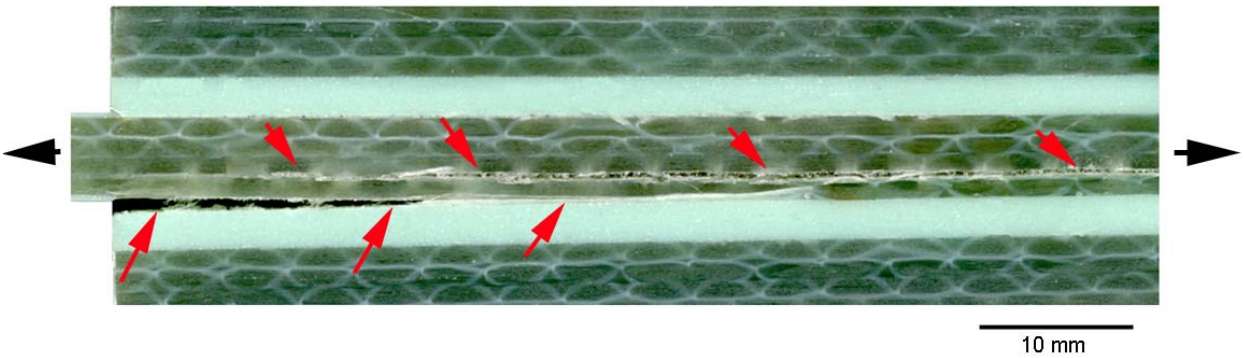

Figure 5. Photograph of crack transition from adhesive into laminate interior, symmetrical CLS geometry, 2.4 mm thick adhesive ADH-1, crack growth left to right.

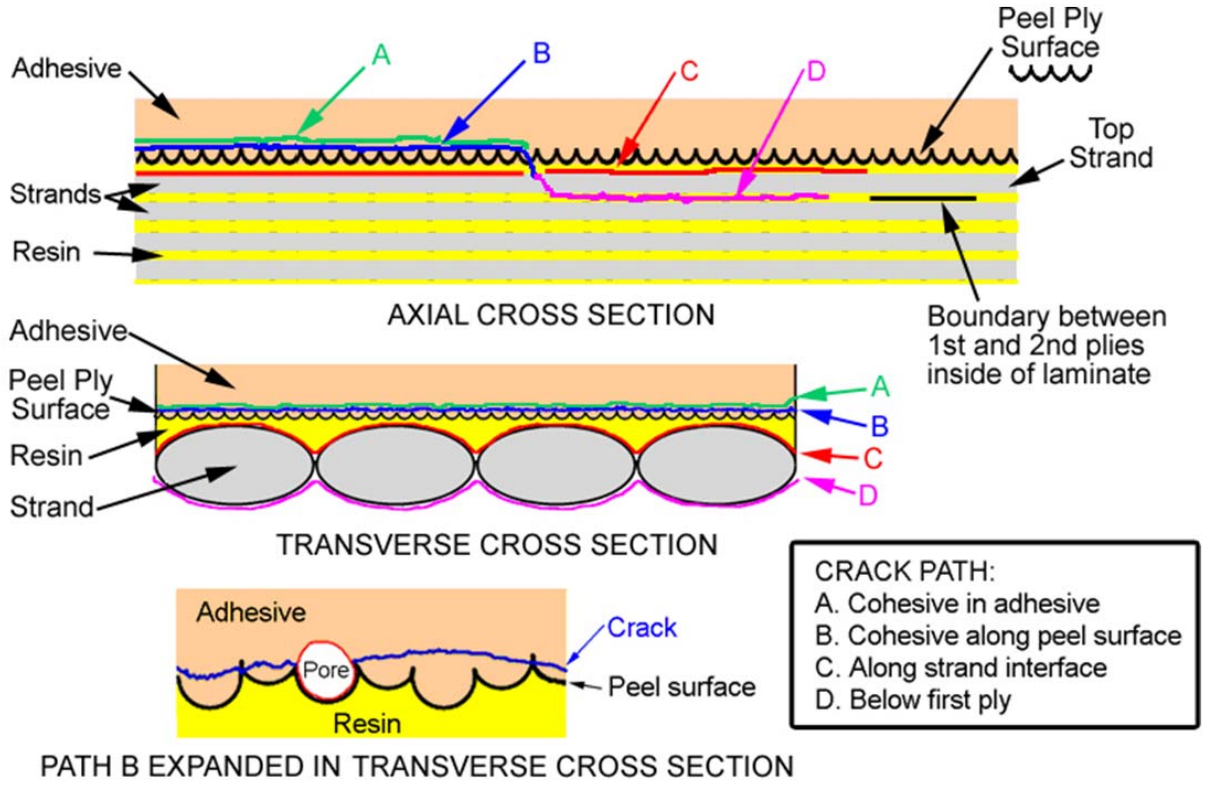

Figure 6. Schematics of local crack growth paths in axial and transverse directions (possible transitions shown on axial section, crack growth left to r): path A, ductile, cohesive within the adhesive, typical of adhesive ADH-6; path B, cohesive within the adhesive, but associated with micro-fracturing along laminate resin peel ply surface, typical of ADH-1; path C, along the laminate strand interface, typical of ADH-5 throughout, and other adhesives after transition; and path D, within the laminate, below ply which is adjacent to adhesive.

Figures 10-15 give SEM micrographs of fracture surfaces. As noted above, cracks in the most brittle adhesive, ADH-1, which also contains short glass fibers, propagated primarily along path B, sometimes transitioning to path C at longer lengths. Fracture surfaces for the as molded peel-ply surface and a path B crack are shown in Figures 10 and 11 at similar scale. The mode II component to the crack forces it to the laminate interface area[3]. The zone along the peel-ply contains many small pores and oriented short fibers from the adhesive, which produce extensive sub-crack initiation, coalescing into the main crack (Figure 7). The complex fracture pattern produces rough, high energy surfaces, so that the ADH-1 adhesive, which has the lowest G_{Ic} in pure mode I, has the highest crack resistance in the CLS test, shown later. The surface roughness is much greater for ADH-1 in mixed mode than pure mode I DCB with the crack in the mid-thickness (compare Figures 11 and 12, taken at the same magnification). The fracture surface features for crack path B, Figure 11, and the corresponding hackle formation in Figure 7, correlate to the spacing of the peel-ply features in Figure 10.

Cracks in mixed mode for the intermediate toughness adhesive, ADH-5, propagated along path C (Figure 13). Occasional chunks of resin and adhesive up to the peel ply surface can be seen where there are local pores on the peel ply surface, as near the center of the micrograph in Figure 13. The toughest adhesive, ADH-1, generally fails along path A, just inside the adhesive, similar to path A, with significant porosity associated with the peel-ply pattern for this hand mixed adhesive case (Figure 14). At longer crack lengths for the CLS specimens, a transition to path C is observed.

Crack growth paths under both fatigue and static loading were similar for each adhesive. A reversed loading fatigue crack surface for adhesive ADH-1 is given in Figure 15. This micrograph indicates a mixture of paths B and C. Mixtures of paths A and C were observed on adhesive ADH-6 fatigue crack surfaces. ADH-5 fatigue cracks remained in path C throughout.

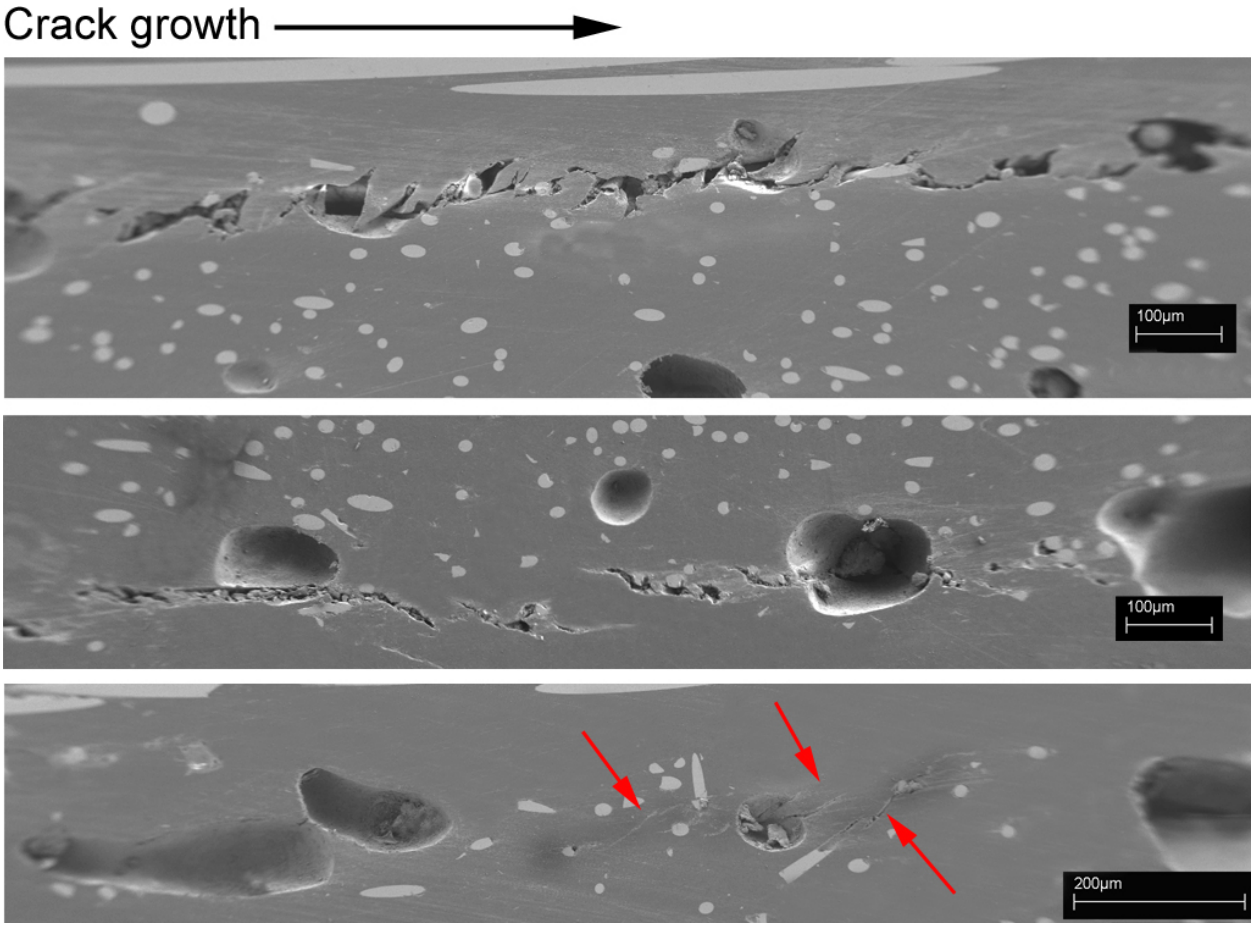

Figure 7. SEM micrographs of crack tip area, static CLS specimens with adhesive ADH-1, crack path B, crack growth left to right: fully cracked, partial shear displacement (top, crack 1a); mostly cracked (middle, crack 1b); and local micro-cracking at arrows ahead of tip at fibers and pores (bottom, crack 1a).

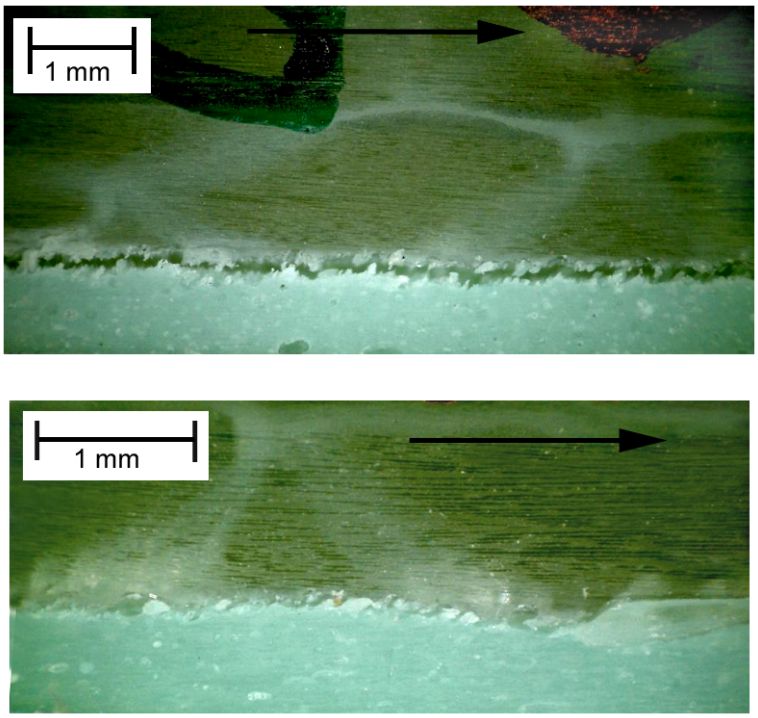

Figure 8. Optical micrographs of static crack paths with laminate strand and stitching visible on top, adhesive on bottom: ENF specimen, path B, crack growth left to right (top) and CLS specimen with steel showing transition from path B to path C on right end, crack growth left to right (bottom); adhesive ADH-1.

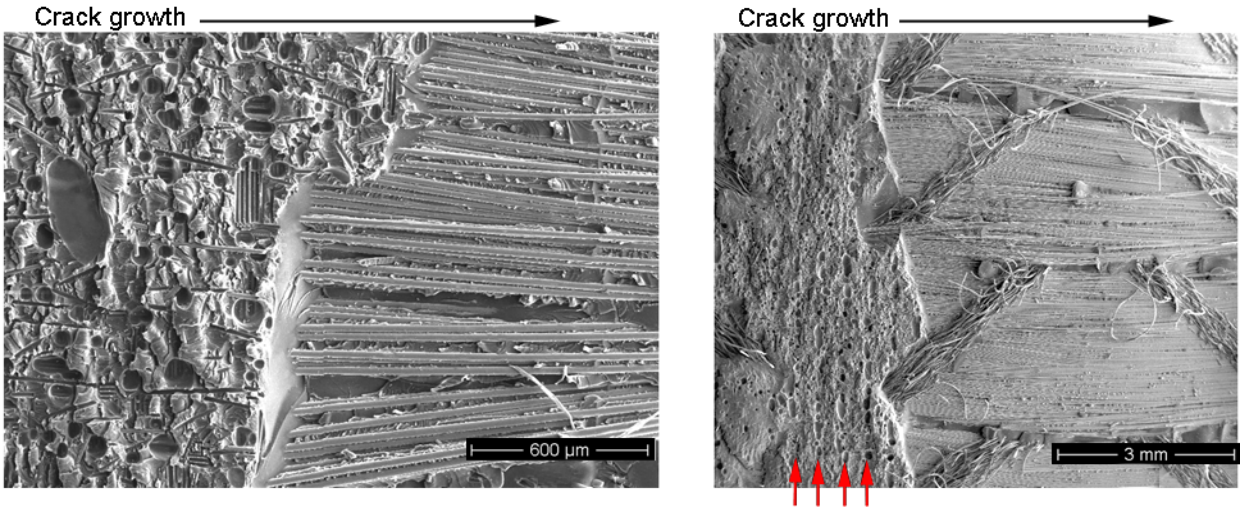

Figure 9. SEM micrographs of typical crack path transitions from path B to C in two MMB specimens, adhesive ADH-1, crack growth left to right. Low magnification fracture surface on right shows rows of pores on left side whose spacing corresponds to the peel-ply pattern dimension, and possible interaction of transition crack with fabric strand stitching (arrow).

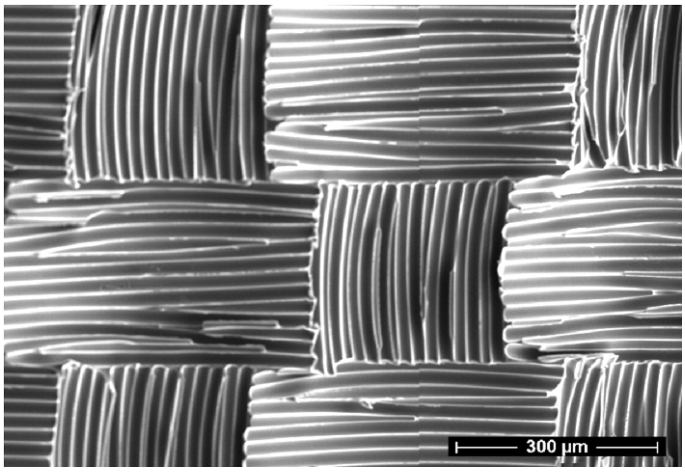

Figure 10. Laminate peel-ply surface as-molded.

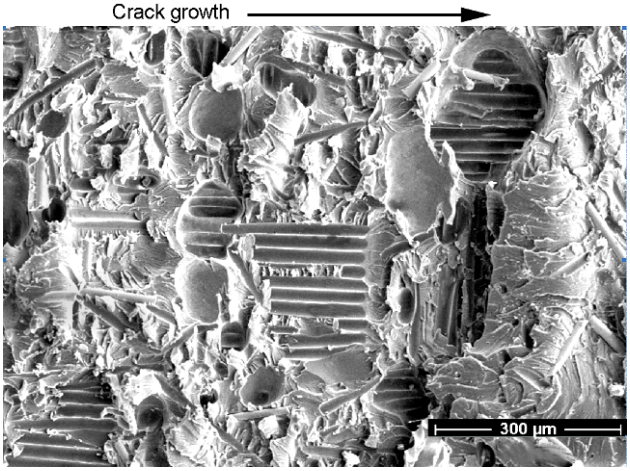

Figure 11. Path B showing fracture through pores over peel ply and through adhesive, ADH-1, static test, looking toward laminate side.

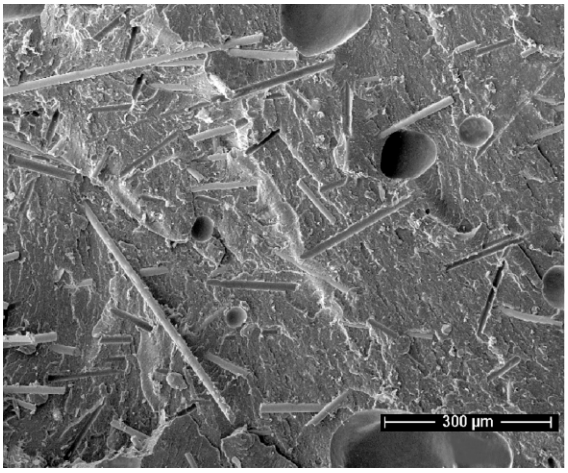

Figure 12. Static fracture surface of ADH-1, DCB test, crack growth at mid-thickness left to right, showing relatively smooth surface compared to Figure 11, with pores and short fibers.

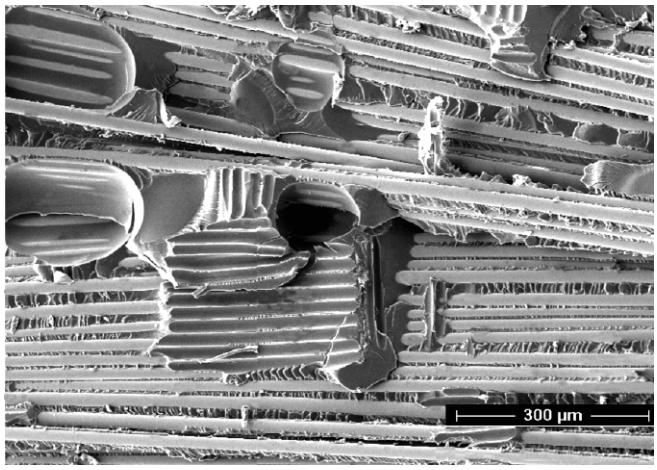

Figure 13. Crack path C, along reinforcement surface, with resin patch showing peel-ply imprint at pore (center), static CLS test, ADH-5, crack growth right to left.

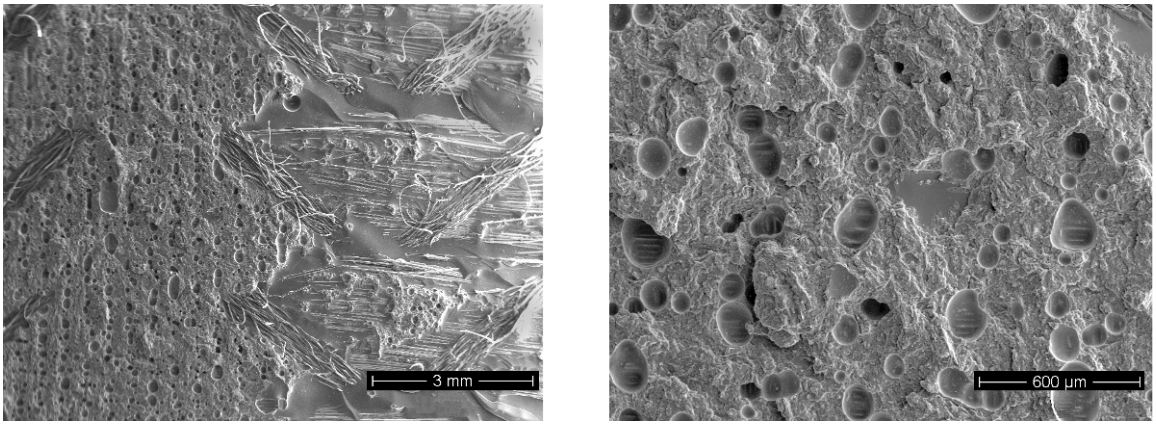

Figure 14. Crack Path A, cohesive near the interface, showing transition to path C (left), crack growth left to right, static CLS test with adhesive ADH-6.

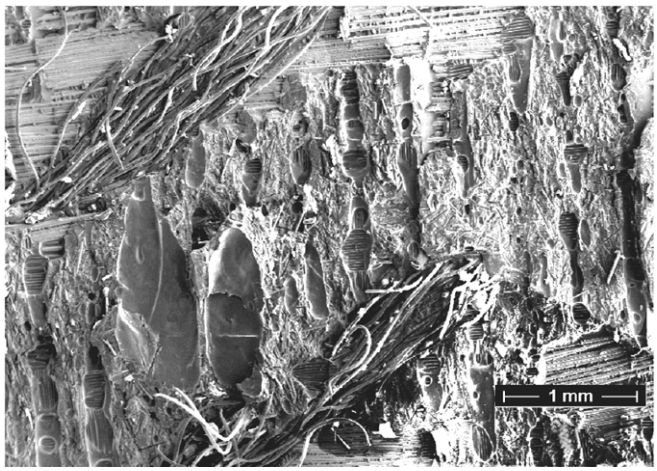

Figure 15. Low magnification reversed loading fracture surface looking toward laminate side, showing transitional characteristics of crack paths B (patches of fractured adhesive) and C (growth along glass strand surface inside laminate, also showing polyester fabric stitching), crack growth left to right, ADH-1, R = 0.1, CLS test.

IV. Test Results

A. Mixed Mode Bending Static Tests

As noted above, for many different geometries, cracks tend to transition from the adhesive (paths A and B), into the strand surface (Figure 9) or the laminate interior (Figure 5). Resistance to propagation is then governed by the laminate delamination resistance (interior laminate) or the similar resistance to separation of the laminate surface resin from the strands (laminate surface). The strand structure of most infused laminates creates matrix rich areas between strands which penetrate through the ply, and are separated from the strands as part of the crack growth process (Figure 7, path C). As a comparison to the adhesive fracture resistance, which follows, a typical dataset for mixed mode interlaminar fracture is given in Figure 16. The various SERR values are calculated from MBT, Eq. 1-7, with critical initial crack propagation loads determined as in Figure 3. Figure 16 is a plot of the total calculated SERR at initial crack growth, G_T (= G_I + G_{II}) vs. the fraction of G_{II} at the test condition, G_{II}/G_T. G_{II}/G_T equals G_{Ic} for the DCB test (G_{II} = 0) and equals G_{IIc} for the ENF test (G_I = 0).This laminate is similar to the adherends in the adhesives study except for the resin, which is SP Systems Prime 20LV, a similar infusion epoxy to that in the adhesives study. Tests were the same as those illustrated in Figure 2. The data indicate much higher mode II toughness, G_{IIc}, compared with mode I G_{Ic}; mixed mode cases are significantly tougher in terms of total strain energy release rate than G_{Ic} as the mode II contribution increases. This trend is typical of relatively brittle resin laminates which show the hackled growth pattern discussed previously when a significant mode II contribution is present[16].

Relative to Figure 16, pure G_{Ic} and G_{IIc} values for the adherend laminate system used here are similar[1], 303 J/m^2 and 3446 J/m^2, respectively at V_f = 0.60, for the same $0^o/0^o$ interface. If the fabric backing to backing interface is cracked, the G_{IIc} value is reduced to 1887 J/m^2, as the backing creates a more nearly flat crack surface which doesn't follow the strand surfaces. Delamination results for other laminates may vary; biax (±45) interfaces with RTM polyester resin laminates showed higher G_{Ic} and G_{IIc} compared to $0^o/0^o$ interfaces in an early study, apparently related to extensive resin cracking away from the immediate crack interface[17].

MMB static test results for the adhesive joints in Figure 2 are given in Figure 17 (2.4 mm thick adhesive ADH-1). The data are presented for MBT calculations, Eq. 1-7, and finite element analysis (FEA) using the VCCT method[7] of calculation for the strain energy release rates. The two calculation procedures are in general agreement for this series of tests. As noted earlier, crack propagation for these tests became unstable after a few mm of growth, transitioning from path B to path C, Figures 6 and 9. Only the pure mode II, ENF tests showed stable growth for the order of 20-30 mm. All mixed mode and pure mode II cracks remained in the top (compression side) interface as indicated in Figure 2; if the starter crack film was located on the bottom interface, the growing crack would kink to the upper interface.

The trend of the data in Figure 17 for the adhesive joint is generally similar to that for laminate delamination in Figure 16. The adhesive G_{Ic} value (G_T at G_{II}/G_T = 0) is higher, but the mixed mode G_T increases less rapidly as the mode II contribution increases, relative to laminate delamination. G_{IIc} values (G_{II}/G_T = 1) for both test series fall in a similar range. The several G_{Ic} values shown represent variations of the starter crack for the DCB test. When the Teflon film is positioned near mid-thickness of the adhesive, the lowest G_{Ic} values are obtained. G_{Ic} is increased when the starter film is positioned at the top interface, and is highest when the starter crack is produced by mixed mode loading at G_{II}/G_T = 0.55, again at the top interface. When the starter crack is at the interface, subsequent mode I propagation is away from the interface, into the adhesive mid-thickness. Also shown on the plot are results for different adherend thicknesses, 3.9 (0_3) and 5.0 mm (0_4). The thicker adherends produced somewhat lower G_{Ic} and G_{IIc} values.

FEA analysis includes the adhesive geometry and properties, while the MBT Equations 1-7 do not, as noted earlier. The FEA calculated results generally follow the MBT values in trend; minor differences in mode mixity are not shown on Figure 17. The FEA calculated DCB G_{Ic} is 34% lower than the MBT value, but GIc values for the crack near the interface are within 10% of the MBT values. The FEA results show a 2% mode II component to the DCB SERR with the crack near the interface. The symmetric CLS specimen is similar to the un-symmetric case in Figure 1, but with additional adhesive layer, laminate adherend, with notch, to create a symmetric sandwich with the single thickness of un-notched laminate adherend in the mid-thickness (100 mm long, no steel). The first crack to form grew unstably after a very short distance of stable growth. SERR values were calculated by FEA.

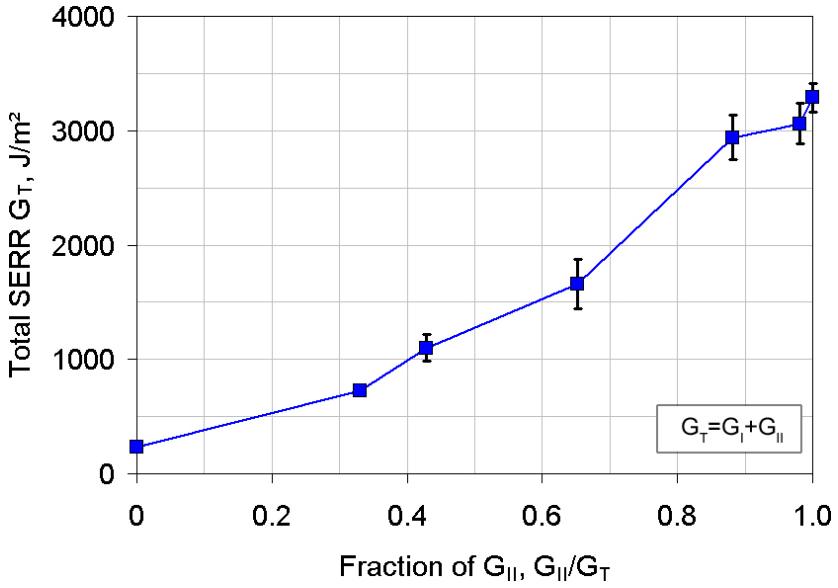

Figure 16. Mixed mode bending static test average results for laminate delamination resistance, unidirectional infused Vectorply ELT-5500 glass fabric with SP Systems Prime 20 LV epoxy, V_f = 0.51[1].

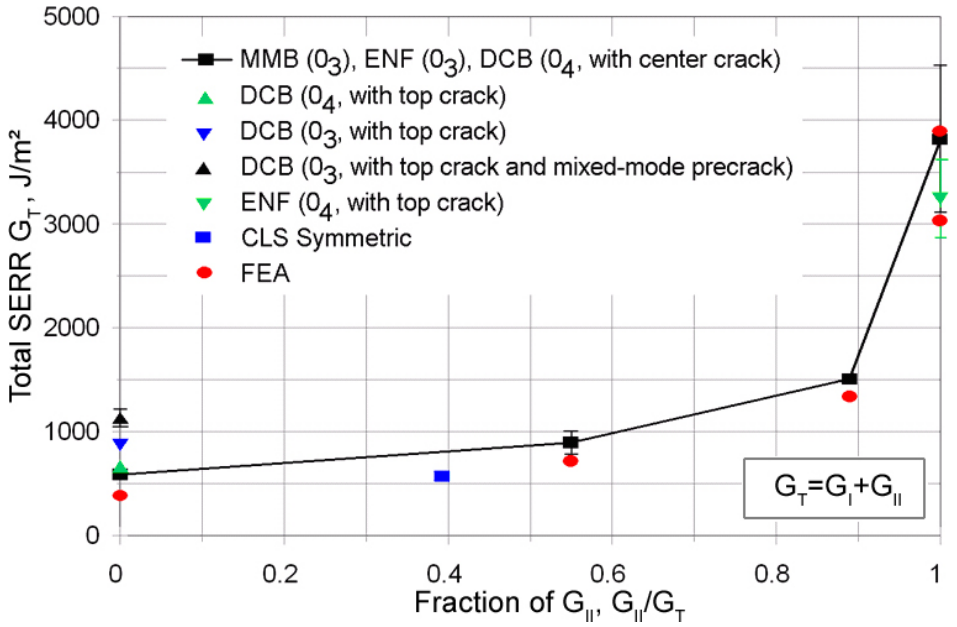

Figure 17. Mixed mode bending static test results for crack growth resistance of 2.4 mm thick ADH-1 adhesive joints: modified beam theory calculations (Eq. 1-7), comparison to FEA calculations from VCCT. Legend indicates laminate adherend thickness: 0_3, three plies, 0_4, four plies, starter crack at the top interface in Fig. 1, or center of adhesive (DCB); or MMB starter crack for DCB case.

B. Cracked Lap Shear Static Tests

Static crack growth results for the CLS specimens with the baseline adhesive are given in Figure 18 as the critical load for propagation, Pc, vs. crack length, a. Cracks were grown from the notch with no starter crack All cracks propagated in a stable manner along path B. When Teflon film starter cracks of differing length or a fatigue starter

crack were used (Figure 19), the results were similar, with the propagation load rising rapidly, approximately to join trend line from Figure 18. The fatigue crack tip was grown at Pmax/Pc of 0.40. The method of crack formation does not appear critical, and severe R-curve effects (increasing crack resistance with crack extension[18]) are not evident. The effects of type of peel-ply used to form the laminate surface, and the mixing method are shown in Figure 20. Little effect of peel ply type is evident; all cracks followed path B. Hand mixing appeared to result in more unstable crack jumps (dashed line), possibly associated with larger pores.

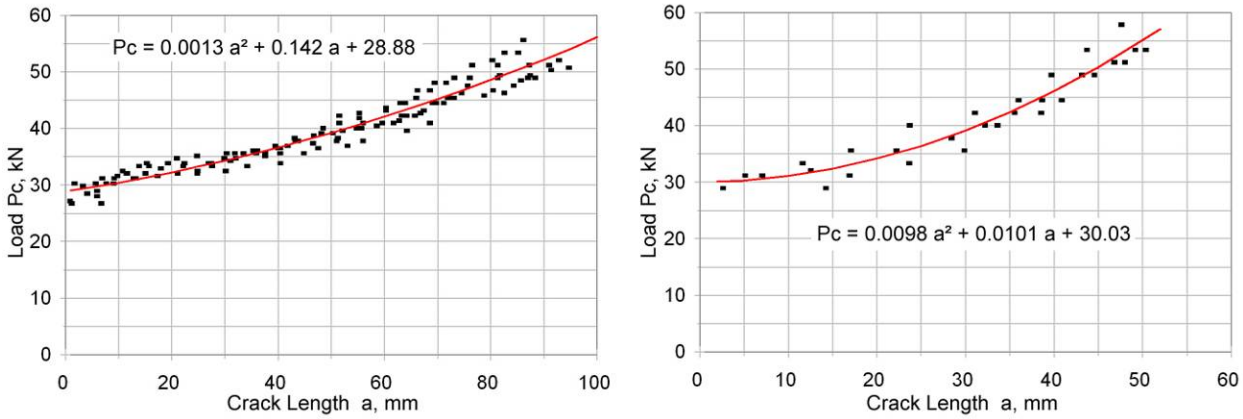

Figure 18. Static critical load vs. crack length, (a) 100 mm CLS with steel (left) and (b) 50 mm without steel, (right); adhesive ADH-1, crack growth from machined notch.

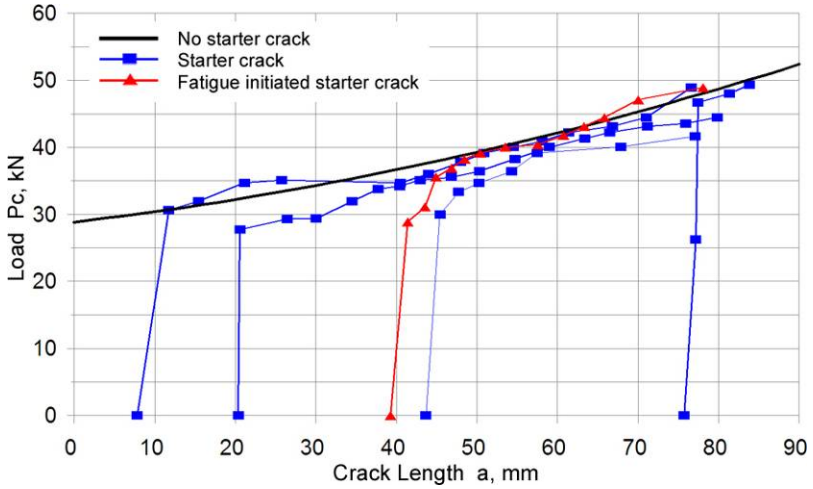

Figure 19. Static critical load vs. crack length, effect of starter crack release film length (blue) and fatigue crack length (red) compared to trend from Figure 18 (a) with no starter crack (black), long CLS with steel.

C. Cracked Lap Shear Fatigue Tests

Fatigue crack growth testing was conducted at 2-4 Hz under load control at R-values (R = min load/max load) of 0.1 (tensile-tension) and -1 (reversed loading). Crack length was monitored periodically at low magnification on a "white-out" coated surface. Individual tests were run at a constant Pmax in most cases, so the crack growth data tend to fall in groups related to the value of Pmax. Figure 21 gives the crack growth rate, da/dN, as a function of Pmax/Pc on a log-log plot for long CLS specimens with steel and short specimens without steel. Points plotted are for individual measured crack length intervals, da, corresponding to the associated cycle interval, dN. The data are separated by crack length interval, as the mode mixity varies with crack length, discussed later. While most mixed mode testing is done for a relatively constant mode mixity, Reference 8 reports results for a single-lap geometry with varying mode mixity along the crack path. There is an apparent separation with crack length of some of

datasets under reversed loading, with shorter cracks propagating more slowly than longer cracks at the same Pmax/Pc ratio, for shorter cracks with the long CLS with steel geometry under reversed loading. Data for other cases do not separate clearly by crack length. Data for reversed loading mostly fall above data for tension-tension, indicating about 10x faster crack growth under reversed loading at the same Pmax/Pc ratio for both specimen geometries. Crack growth is also somewhat faster for the long specimen geometry with steel than for the short specimens at similar Pmax/Pc ratios. These results are considered further in the final section.

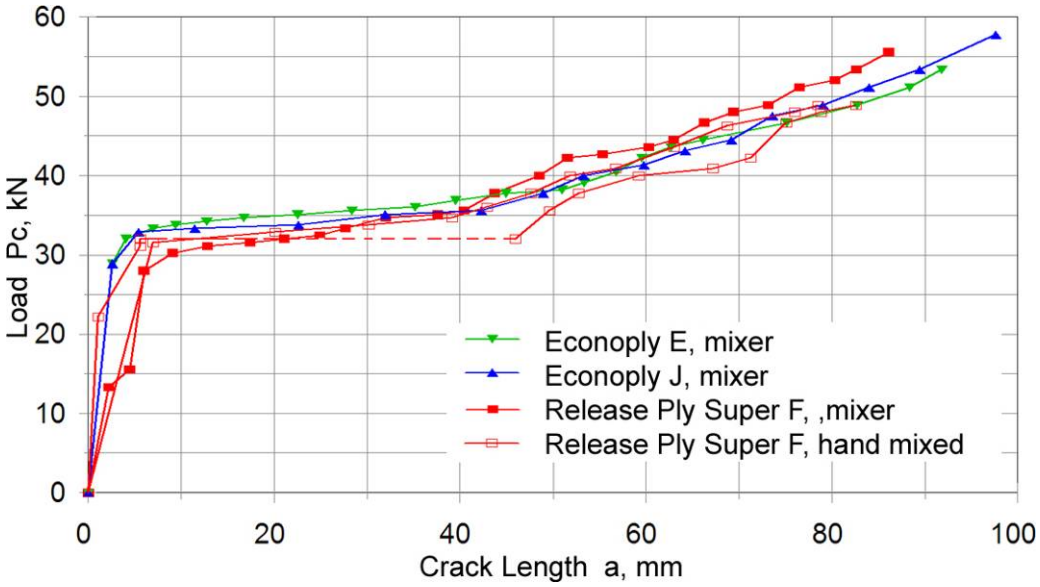

Figure 20. Effect of laminate peel-ply type and adhesive mixing method (machine mixed unless noted) on static crack growth resistance from machined notch; dashed line indicates unstable crack jump.

D. Comparison of Different Adhesives

This section compares the three adhesives used in this study, ADH-1, ADH-5 and ADH-6, for a limited range of tests; the adhesive thickness was 3.8 mm for these tests, compared with the 2.4 mm used for the remainder of the tests, which affects the results. Table 2 gives mode I G_{Ic} results from DCB tests; data are reduced using Eq. (1). The DCB results in Table 1 show adhesive ADH-6 at much higher toughness than ADH-1, with ADH-5 intermediate. Crack starter films were located at mid-thickness, and cracks for the three adhesives tended to stay in the mid-thickness area, with the most significant undulation for ADH-5. Crack growth in mode I is mid-thickness, so this test provides a measure of the inherent adhesive toughness.

Cracks in the CLS mixed mode test are forced near one interface by the shear stress component, which gives direction to the stress field so that cracks propagating under the local maximum tensile stress grow at some angle to the crack direction[3]. Static (Figure 22) and fatigue (Figure 23) data using the short specimen geometry without steel are now more similar for the three adhesives compared with Table 1; in fact, the static loads for the most brittle system, ADH-1, are the greatest of the three. The local mode of crack growth on path B (Figures 6 and 11) produces a rough fracture surface and high crack resistance for brittle adhesives compared to path C in the strand interface (Figure 12). The data for ADH-1 fall slightly below the trend in Figure 18 for ADH-1 with the thinner 2.4 mm thick adhesive, as expected[1-3].

Fatigue crack growth in terms of Pmax/Pc is similar for ADH-1 and ADH-6 on crack paths B and A, respectively; slightly poorer for ADH-5 on path C.

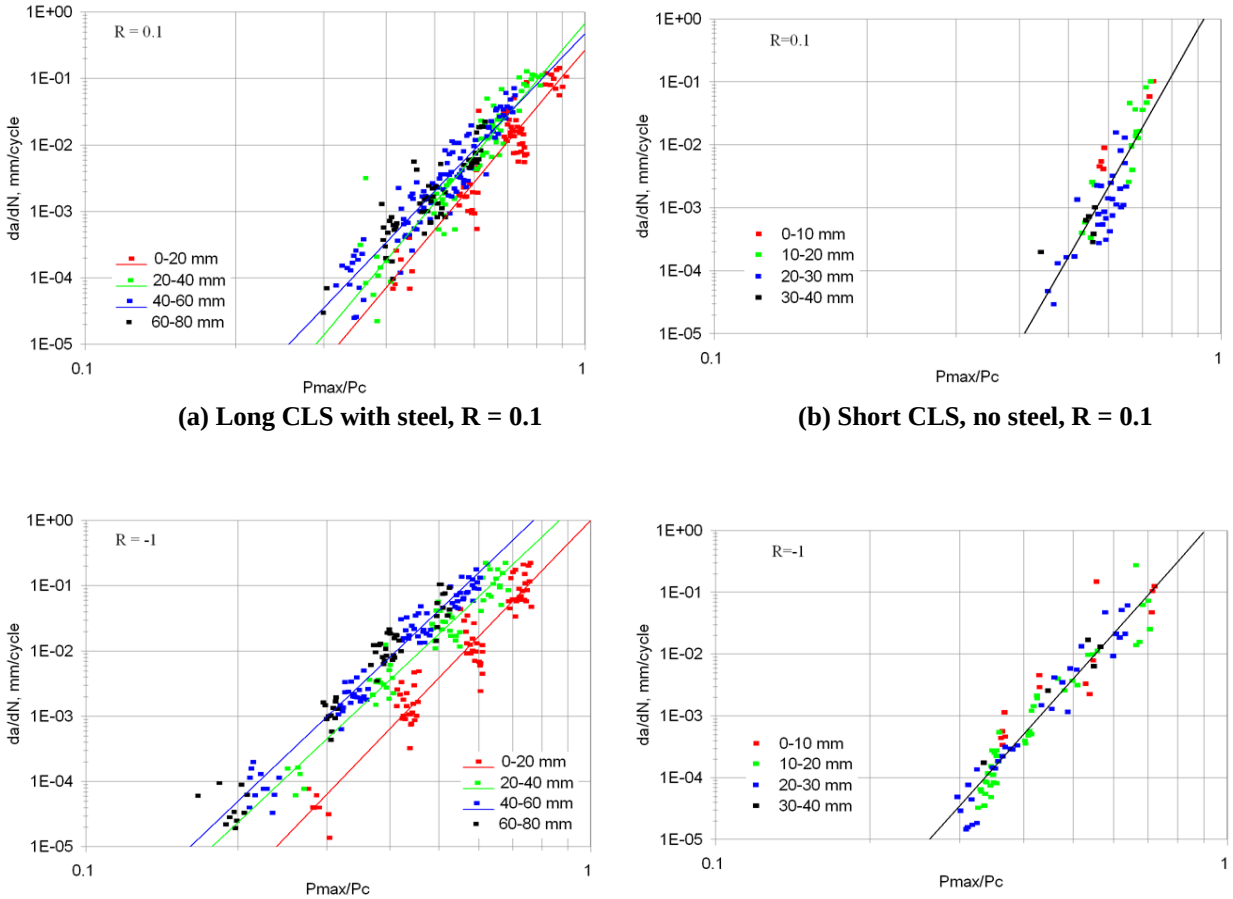

(a) Long CLS with steel, R = 0.1

(b) Short CLS, no steel, R = 0.1

(c) Long CLS with steel, R = -1

(d) Short CLS, no steel, R = -1

Figure 21. Fatigue crack growth data in terms of P_{max}/P_c for CLS specimens at R = 0.1 and -1. Data differentiated by crack length.

Table 1. Line Fit Equations for Figure 21.

Coupon	Figure	Crack Length Range, mm	Best Fit Equation, mm/cycle
Long CLS with steel, R = 0.1	21 (a)	0 – 20	$da/dN = 0.27\ (Pmax/Pc)^{8.99}$
		20 – 40	$da/dN = 0.67\ (Pmax/Pc)^{8.98}$
		40 – 80	$da/dN = 0.47\ (Pmax/Pc)^{7.89}$
Short CLS, R = 0.1	21 (b)	0 – 40	$da/dN = 2.96\ (Pmax/Pc)^{14.14}$
Long CLS with steel, R = -1	21 (c)	0 – 20	$da/dN = 0.99\ (Pmax/Pc)^{8.03}$
		20 – 40	$da/dN = 2.77\ (Pmax/Pc)^{7.26}$
		40 – 80	$da/dN = 6.70\ (Pmax/Pc)^{7.35}$
Short CLS, R = -1	21 (d)	0 - 40	$da/dN = 2.45\ (Pmax/Pc)^{9.27}$

Table 2. DCB adhesive G_{Ic} results, 3.8 mm adhesive thickness[2].

Adhesive	Average G_{Ic}, J/m^2
ADH-1	581
ADH-5	938
ADH-6	1626

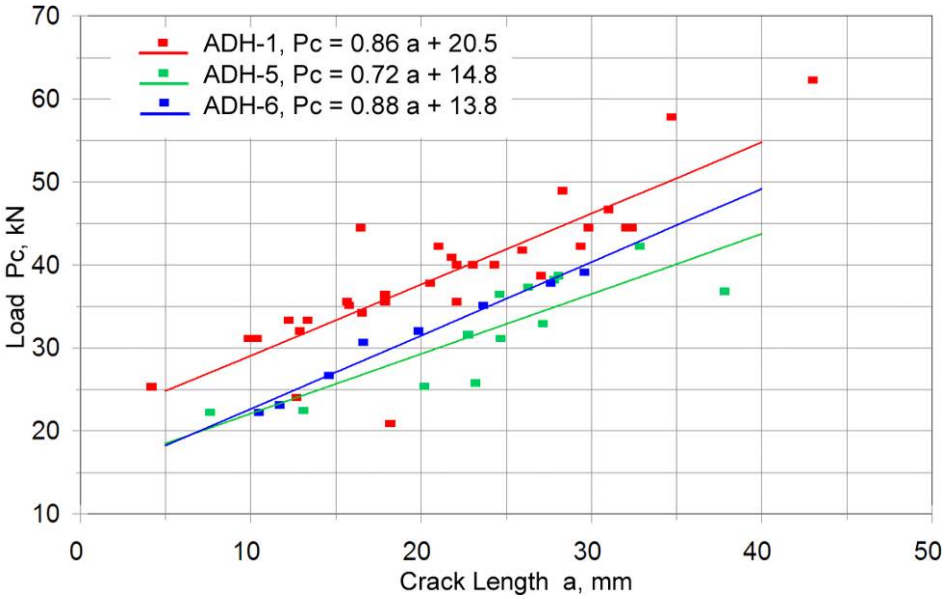

Figure 22. Static P_c values vs crack length for three adhesives (short CLS specimen, no steel, 3.8 mm adhesive thickness.)

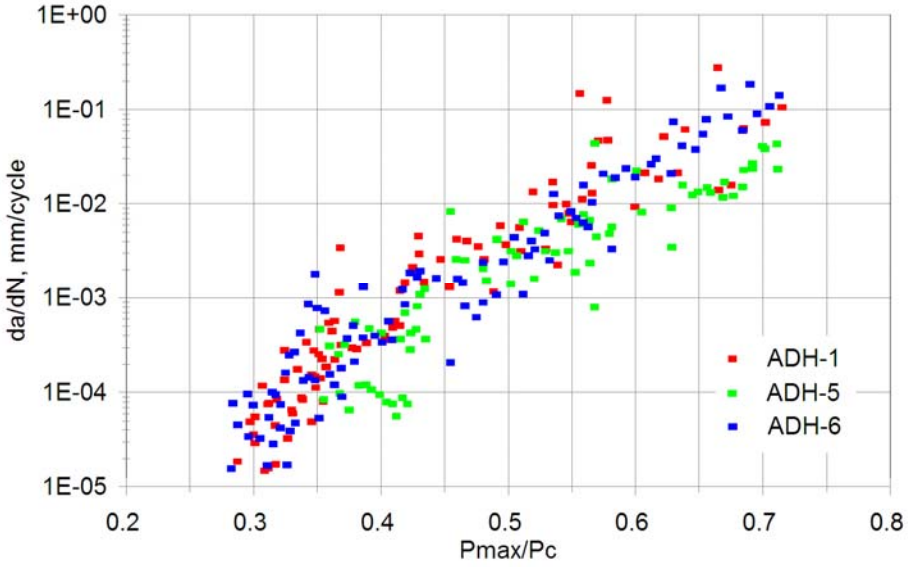

Figure 23. Comparison of reversed loading fatigue crack growth rates for three adhesives (short CLS specimen, no steel, 3.8 mm adhesive thickness).

E. Discussion

The CLS specimen geometries shown in Figure 1 proved very functional in an experimental sense: they were convenient to prepare and test using the grip system in Figure 1(b), crack growth was generally stable, following paths A, B or C illustrated in Figure 6 for the three adhesives studied, and results were reproducible, with significant but acceptable scatter. Various FEA efforts to date show mode mixities (G_{II}/G_T) in the approximate ranges of 0.4-0.6 for the short geometry and 0.5-0.9 for the long geometry with steel. The associated FEA study is in progress, exploring the applicability of VCCT and cohesive zone modeling to these joints. Difficulty has been encountered in obtaining consistent results for the CLS and MMB geometries, apparently related to grip fixity effects for the non-symmetric CLS test (the symmetric CLS specimen gives similar results to the MMB tests when analyzed by VCCT, but crack growth is unstable, Figure 17).

V. Conclusions

This study has explored static and fatigue crack growth in thick adhesive joints with fiberglass laminate adherends, for three adhesive systems with a broad range of G_{Ic} values. Data have been presented for mixed shear and opening mode loading conditions, and for tension-tension and reversed loading fatigue. The several versions of the CLS test geometry allow fully reversed and compression loading, in addition to tension. Widely used flexural test geometries (DCB, MMB, and ENF) have been used to obtain static crack growth properties and as a baseline for comparison to the CLS test results. Crack paths and damage characteristics have been characterized using microscopy for CLS and flexural geometries.

Cracks were shown to propagate along four potential paths depending on adhesive and geometry: a. cohesive in the adhesive, mid adhesive for pure mode I, but otherwise near one laminate adherend interface; b. cohesive in the adhesive, but partially involved with cracking from the laminate resin peel-ply surface features; c. inside the laminate resin, along the top fiberglass strand surface; and d. inside the laminate, below the top (fabric) ply. Transitions from (a) and (b) to (c), involving unstable growth, were observed for flexural geometries after a short period of stable crack growth under static loading. Stable growth was observed for most CLS tests. The crack tip area for the more brittle adhesive (ADH-1) showed a zone of one to two mm ahead of the fully formed crack tip, where micro-cracking and hackling damage were present; the damage extended for the order of 0.1 to 0.2 mm into the adhesive thickness from the interface.

Static test results for the flexural geometries followed a trend of the total SERR, G_T, with mode mixity, which was similar to interlaminar cracks in a similar laminate to the adherends, with increasing G_T as the mode II component increased; SERR levels were of generally similar magnitude. Thus, comparable static crack resistance is expected for cohesive cracks in the adhesive, or for cracks which transition into the laminate surface or interior. The CLS static crack growth resistance was insensitive to the type of peel-ply, and to crack starter method, whether grown from the notch, from a Teflon starter film, or from a mixed mode fatigue crack (Figure 19).

Fatigue crack data were obtained for two CLS specimen geometries for adhesive ADH-1 under tension-tension and reversed loading. Crack growth rates, da/dN, were represented as the maximum load normalized by the static critical load at the same crack length. Cracks followed a power law relationship, propagating more rapidly under reversed loading than tension-tension for the same Pmax/Pc. Data were separated according to crack length, presumably reflecting an increased mode II component for longer cracks.

Comparisons of the three adhesives indicate adhesive ADH-6 with a much higher static G_{Ic} from DCB tests with the crack at mid-thickness, compared to ADH-1, and with ADH-5 intermediate. Mixed-mode CLS tests showed generally similar crack resistance for all three adhesives, highest for ADH-1, with cracks propagating near the interface. CLS fatigue cracks propagated at a similar speed for the same Pmax/Pc ratio for all three adhesives.

General applicability of the CLS results requires adequate modeling of the test geometry.

References

[1]Mandell, J. F., Samborsky, D.D., Agastra, P., Sears, A.T. and Wilson, T.J., "Analysis of SNL/MSU/DOE Fatigue Database Trends for Wind Turbine Blade Materials," 2010, Sandia Contractor Report SAND2010-7052 (www.coe.montana.edu/composites/).

[2]Sears, A.T., Samborsky, D.D., Agastra, P. and Mandell, J.F., "Fatigue results and analysis for thick adhesive notched lap shear test," 2010 AIAA SDM, Wind Energy Session, Orlando, AIAA-2010-2821.

[3]Dillard, D.A., Advances in Structural Adhesive Bonding," CRC Press, New York, Woodhead Publishing Ltd. 2010, Ch. 13.

[4]Choupani, N., JAST, 3 (2006) 185-193.

[5]Bing, Q. and Sun, C. T., "Effect of Transverse Normal Stress on Mode II Fracture Toughness in Fiber Composites," 16th Inter. Conf. Composite Materials, Kyoto, 2007.

[6]Nijssen, R. P. L., Westphal, T., Stmmes, E., Sari, J., "Strength and Fatigue of Wind Turbine Rotor Laminates and Substructures," 2010 AIAA/ASME Wind Energy Symposium, AIAA- 2010-1189.

[7]Rybicki E. F. and Kanninem M. F., Eng. Fract. Mech., 9 (1977) 931–938.
[8]Quaresimin, M., and Ricotta, M., Composites Sci. and Tech., 66 (2006) 647-656.
[9]Mall, S. and Yun, K.T., J. Adhesion, 1987, vol. 23, pp. 215-231.
[10]Li, S., Thouless, M. D., Waas, A. M., Schroeder, J. A., and Zavattiere, Experimental Fracture Mechanics, 73 (2006) 64-78.
[11]De Moura, M. F. S. F., Goncalves, J. P. M., Chousal, J. A. G., Campilho, R. D. S. G., Int. J. Adhesion and Adhesives, 28 (2008) 419-426.
[12]Chai, H., Int. J. Solids and Structures, 40 (2003) 6023-6042.
[13]Reeder, J. R. and Crews, J. H. J., AIAA Journal, 28 (1990) 1270-1276.
[14]Mandell, J.F. and Samborsky, D.D., "DOE/MSU Fatigue of Composite Materials Database, 2010 update (www.sandia.gov/wind/other/973002upd0309.pdf).
[15]Russell, A. J. and Street, K. N., in "Delamination and Debonding of Materials, STP 876," W. S. Johnson, Ed., ASTM, Phil., 1985,349-370.
[16]Corleto, C. R. and Bradley, W. L., in Composite Materials: Fatigue and Fracture, Second Volume, ASTM STP 1012, P. A. Lagace, Ed., ASTM, Phil., 1989, 201-221.
[17]J.F. Mandell, D.D. Samborsky, and D.S. Cairns, "Fatigue of Composite Materials and Substructures for Wind Turbine Blades," Contractor Report SAND2002-0771, Sandia National Laboratories, Albuquerque, NM, (2002).
[18]Broek, D., Elementary Fracture Mechanics, Ch. 8, 4th Ed., Martinus Nijhoff, Dordrecht, The Netherlands, 1986.